JACS
JOURNAL OF THE AMERICAN CHEMICAL SOCIETY
Article
pubs.acs.org/JACS

Description and Role of Bimetallic Prenucleation Species in the Formation of Small Nanoparticle Alloys

Lauren E. Marbella,[†] Daniel M. Chevrier,[§] Peter D. Tancini,[‡] Olabobola Shobayo,[‡] Ashley M. Smith,[†] Kathryn A. Johnston,[†] Christopher M. Andolina,[†] Peng Zhang,[§] Giannis Mpourmpakis,[‡] and Jill E. Millstone*[,†]

[†]Department of Chemistry and [‡]Department of Chemical Engineering, University of Pittsburgh, Pittsburgh, Pennsylvania 15260, United States

[§]Department of Chemistry, Dalhousie University, Halifax, NS B3H 4J3, Canada

Supporting Information

ABSTRACT: We report the identification, description, and role of multinuclear metal−thiolate complexes in aqueous Au−Cu nanoparticle syntheses. The structure of these species was characterized by nuclear magnetic resonance spectroscopy, mass spectrometry, X-ray photoelectron spectroscopy, and X-ray absorption spectroscopy techniques. The observed structures were found to be in good agreement with thermodynamic growth trends predicted by first-principles calculations. The presence of metal−thiolate complexes is then shown to be critical for the formation of alloyed Au−Cu architectures in the small nanoparticle regime (diameter ∼2 nm). In the absence of mixed metal−thiolate precursors, nanoparticles form with a Cu−S shell and a Au-rich interior. Taken together, these results demonstrate that prenucleation species, which are discrete molecular precursors distinct from both initial reagents and final particle products, may provide an important new synthetic route to control final metal nanoparticle composition and composition architectures.

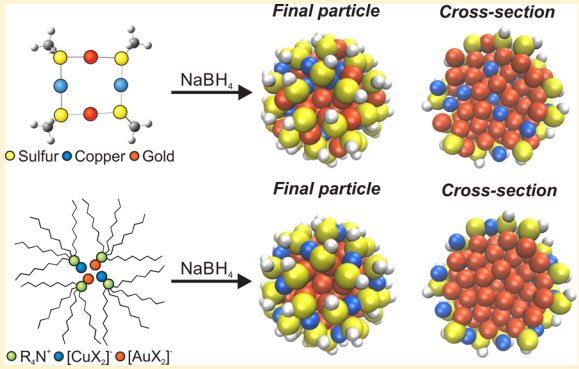

INTRODUCTION

Both the composition and relative position of atoms in bimetallic nanoparticles (NPs) are crucial determinants in the electronic structure of the resulting materials.[1−3] This electronic structure, especially at the particle surface, significantly impacts emergent properties including catalytic behavior,[4] optical signatures,[5,6] and magnetic phenomena.[7] For example, the presence and position of even a single metal atom substitution have been demonstrated to dramatically influence emergent properties such as particle bandgap and plasmonic features.[8−12] These remarkable structure−property relationships drive an intriguing synthetic holy grail: atom-level control of multimetallic nanostructures.

Yet, developing these molecular mechanisms of nanoparticle formation is challenging because the formation of colloidal metal NPs often involves not only chemical change (e.g., metal cation reduction) but also phase change (i.e., particle nucleation). For example, species distinct from both the initial molecular reagents as well as the final NP architecture have recently been observed during the formation of monometallic noble metal NPs[13,14] as well as during the formation of quantum dots.[15] The existence of these "prenucleation species" is intriguing because it suggests NP formation pathways such as multiple-step nucleation or aggregation-induced particle formation. Ultimately, controlling the structure of these species may lead to major advances in the atom-scale control of particle chemistries and create both new routes to and also types of alloys,[16,17] semiconductor compounds,[18] and other nanoparticle solids.

Here, we report the identification and description of bimetallic metal−thiolate prenucleation species in the aqueous synthesis of thiol-capped bimetallic NPs and demonstrate the impact of these precursors on final NP composition and composition architecture. Specifically, we consider the formation of small (diameter, $d \sim 2$ nm) Au_xCu_yNP alloys. This metal combination is widely studied in both nanoclusters[3,8,19,20] and larger NPs,[21−23] incorporates both noble and 3d transition metals, and is known to exhibit composition-dependent optoelectronic behaviors.[8,11,19,24] Therefore, characterization of molecular mechanisms in these syntheses has the potential to impact a wide variety of synthetic approaches to multimetallic NP formation as well as to enhance our understanding of fundamental chemical phenomena driving metal mixing behavior across length scales.

Received: September 26, 2015
Published: December 15, 2015

DOI: 10.1021/jacs.5b10124
J. Am. Chem. Soc. 2015, 137, 15852−15858

EXPERIMENTAL SECTION

Materials. Hydrogen tetrachloroaurate(III) trihydrate ($HAuCl_4 \cdot 3H_2O$, 99.999%), copper(II) nitrate hemipentahydrate ($Cu(NO_3)_2 \cdot 2.5H_2O$, >99.99%), copper(II) chloride ($CuCl_2$, ≥99%), sodium chloride (NaCl, 99.5%), tetraoctylammonium bromide (TOAB, 98%), *O*-(2-mercaptoethyl)-*O*′-methylhexa(ethylene glycol) (OEGSH, ≥95% oligomer purity, CAS: 651042-82-9), hexanes (98%), toluene (99.8%), absolute ethanol, and dodecanethiol (DDT, ≥98%) were purchased from Sigma-Aldrich (St. Louis, MO). Poly(ethylene glycol) methyl ether thiol (PEGSH, average M_n = 1 kDa) was purchased from Laysan Bio, Inc. (Arab, AL). Deuterium oxide (D_2O, 99.9%), toluene-d_8 (99.5%), benzene-d_6 (99.5%), and ethanol-d_6 (99%) were purchased from Cambridge Isotope Laboratories, Inc. (Tewksbury, MA). All reagents were used as received unless otherwise indicated. NANOpure (Thermo Scientific, ≥18.2 MΩ·cm) water was used to prepare all aqueous solutions. Before use, all glassware, including NMR tubes, and Teflon-coated stir bars were washed with aqua regia (3:1 ratio of concentrated HCl and HNO_3 by volume) and rinsed thoroughly with water. *Caution: aqua regia is highly toxic and corrosive and requires proper personal protective equipment. Aqua regia should be handled in a fume hood only.*

Preparation of Mono- and Bimetallic Prenucleation Species (Aqueous). The preparation of prenucleation species is identical to the first steps of mono- and bimetallic nanoparticle syntheses described previously.[24] Briefly, 188 μL total volume of 20.0 mM $HAuCl_4$ and $Cu(NO_3)_2$ at various initial molar ratios (*vide infra*) were added to 4.29 mL of water. While stirring, 376 μL of 10.0 mM PEGSH solution was added and immediately analyzed by each of the following methods: nuclear magnetic resonance (NMR), X-ray photoelectron spectroscopy (XPS), X-ray absorption spectroscopy (XAS), and matrix-assisted laser desorption ionization-time-of-flight-mass spectrometry (MALDI-TOF-MS) (complete experimental details for each method can be found in the Supporting Information).

Aqueous Au_xCu_yNP Syntheses. The one-phase, room temperature aqueous Au_xCu_yNP synthesis has been described previously.[24] Briefly, 188 μL total volume of 20.0 mM $HAuCl_4$ and 20.0 mM $Cu(NO_3)_2$ at various initial molar ratios were added to 4.29 mL of water. Then, 376 μL of 10.0 mM of PEGSH or OEGSH was added while stirring. Immediately after ligand addition, 450 μL of 20.0 mM $NaBH_4$ was injected to produce Au_xCu_yNPs. The NPs were allowed to age for 1 h prior to purification by washing five times in 30 kDa molecular weight cutoff filters (Amicon Ultra centrifugal filter units, EMD Millipore) at 4000 rcf for 15 min.

Two-Phase Au_xCu_yNP Syntheses. Here, Au_xCu_yNPs were synthesized by a modified Brust−Schiffrin synthesis[25] as described by Tong and co-workers.[26] We further modified the procedure to produce bimetallic Au−Cu nanoparticles. First, 700 μL total volume of aqueous 0.1421 M $HAuCl_4$ and 0.1421 M $CuCl_2$ (at various molar ratios) were added to 10 mL of 0.030 M TOAB in toluene while stirring. The two-phase reaction mixture was heated to 80 °C for 30 min to facilitate phase transfer of metal ion precursor species into the organic phase. The toluene phase changed from clear to red or dark orange, depending on the initial molar ratio of Au:Cu. After 30 min, the aqueous layer was removed, and the reaction mixture containing TOAB and metal salt precursors was allowed to cool to room temperature for an additional 30 min. An aliquot was removed for ICP-MS analysis to determine the total amount of metal transferred to the organic phase.

Once the reaction mixture returned to room temperature, 71.9 μL of neat DDT (density = 0.845 g/mL at 25 °C) was added and stirred for 1 h. The reaction mixture changed from a deep red or dark orange to clear upon addition of DDT (complete color change within 10 s). After 1 h, 1.0 mL of 1.0 M ice-cold, freshly prepared $NaBH_4$ was injected into the rapidly stirring solution and allowed to stir for 4 h before purification.

In order to purify the resulting Au_xCu_yNPs, the organic phase was washed with water (3 × 15 mL). The crude NP product was concentrated by removing the toluene under reduced pressure at 40 °C via rotary evaporation. The crude product was then resuspended in 30 mL of absolute ethanol, sonicated, and placed in the freezer to allow precipitation of the purified DDT-capped nanoparticle product overnight. The precipitate was subsequently washed three times with absolute ethanol and resuspended in hexanes for further analysis (see Supporting Information for full characterization).

RESULTS AND DISCUSSION

Prenucleation Species Identification and Characterization. Aqueous Au_xCu_y nanoparticles are synthesized using four reagents: a thiolated capping ligand, the two metal ion precursors, and a reducing agent. At synthetic concentrations, a mixture of the capping ligand and metal ion precursors was evaluated using 1D ^{1}H NMR and ^{1}H diffusion measurements prior to introduction of the reducing agent (Figure 1). Once

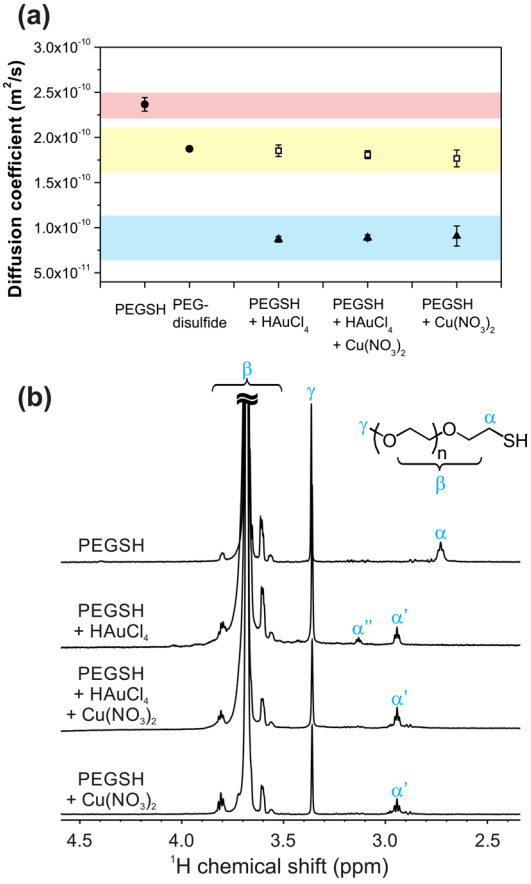

Figure 1. (a) Diffusion coefficient of species from (b) measured by integration of the $(O-CH_2-CH_2)_n$ repeat units of the PEG species, *β*. (b) ^{1}H NMR spectra recorded at 14.1 T of 0.78 mM PEGSH alone in solution and in the presence of 0.78 mM $HAuCl_4$, $HAuCl_4$:$Cu(NO_3)_2$ 50:50, and $Cu(NO_3)_2$ (solvent for all solutions is 90% H_2O, 10% D_2O) at 25 °C.

combined, and in the absence of additional reducing agent, oxidation of the thiol moiety is observed. As may be expected, the extent of thiol oxidation is dependent on both the molar ratio of ligand to metal ion as well as the molar ratio of the two metal ion precursors at constant thiol to total metal ion ratios (see Figure S2). Oxidation of the thiol moiety is indicated by the shift of the ^{1}H triplet from the α-CH_2 group (with respect to sulfur, α) from 2.73 to 2.94 ppm (^{1}H adjacent to a disulfide, α').[27] In all ^{1}H diffusion measurements, the peak labeled α' exhibited a single-exponential decay. However, in all precursor solutions, ^{1}H diffusion decay curves for peak β exhibited a

DOI: 10.1021/jacs.5b10124
J. Am. Chem. Soc. 2015, 137, 15852−15858

biexponential decay (Figure S3), from which two diffusion coefficients could be extracted. One diffusion coefficient corresponds to PEG-disulfide (Figure 1a, open squares), and the other diffusion coefficient corresponds to a higher molecular weight species (Figure 1a, closed triangles). Calibration with molecular weight standards indicates that the mass of the slowest diffusing species is approximately ~4−5 kDa—too large for a PEG-disulfide species alone and consistent with the formation of metal−thiolate structures (Figure 1).

Mass spectrometry analysis of the resulting products supports these assignments. In the case of the monometallic 100% $HAuCl_4$ + PEGSH, a high molecular weight species is observed with a center of mass at 5222.76 m/z that corresponds to the Na^+ adduct of Au_4L_4 (Figure 2, L = PEGSH, calculated m/z = 5222.88). As Cu is added to the precursor solution, the peak center of mass shifts to lower m/z values, consistent with the incorporation of a lighter element. These assignments are supported by control experiments using an oligomer analogue of the PEGSH ligand, where peak shifts correspond directly to the replacement of Au with Cu (Δ133.42 m/z, Figures S6, S8, S17−S20, and Table S2).

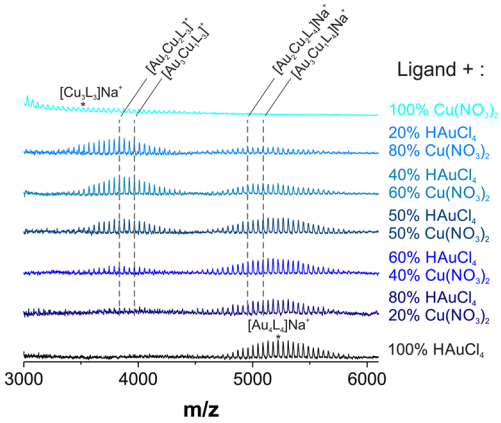

Figure 2. MALDI-TOF-MS of PEGSH in the presence of various molar ratios of $HAuCl_4$:$Cu(NO_3)_2$.

In all bimetallic syntheses described above, the predominant species present are assigned to a tetranuclear, bimetallic complex. To support this structure assignment, metal atom oxidation state and binding environments were analyzed using XPS and XAS. In all cases, when either metal precursor (Au or Cu) is reduced to the +1 oxidation state, the metal atom is bound to sulfur, consistent with the observations and assignments in MS and NMR (see Supporting Information for a detailed discussion on X-ray analyses of precursor solutions). However, we note that for mixed metal solutions both XPS and XAS measurements show that the majority of Cu species remain in the +2 oxidation state after ligand addition (~80−90% remains Cu(II) depending on Au to Cu ratios).

The limited reduction of $Cu(NO_3)_2$ impacts the metal atom ratios within the mixed metal−thiolate prenucleation species and is important in the targeted design of these structures (*vide infra*). For example, at initial molar ratios of 4:1 Cu(II):Au(III), the observed metal−thiolate complexes correspond to Au-rich prenucleation species (Figure 2, Figures S6 and S7). Density functional theory (DFT) simulations help to clarify these observations. When the starting oxidation states of the metals are both +1, a pure Au metal−thiolate complex is the least energetically favorable of the possible complexes, and instead, mixed-metal or Cu-rich species are preferred (Figure S9b). In practice, due to the low concentration of Cu(I) in these reactions, we observe a higher population of Au-rich prenucleation structures. However, even at low concentrations of Cu ions, mixed-metal thiolate complexes form at readily observed concentrations, consistent with DFT predictions (Figure 2 and Figure S6).

Taken together, these results indicate that metal mixing in small NP alloys begins before the nucleation process is initiated. Instead, alloying at this length scale may rely on "premixing" of metals that occurs via formation of multinuclear complexes between metal ion precursors and ligands during the early stages of NP formation. Interestingly, these results are consistent with other examples where mixed metal precursors are crucial to obtain otherwise immiscible metal alloys.[28,29]

Impact of Prenucleation Species on Final Nanoparticle Composition and Composition Architecture. In order to test the hypothesis that the mixed metal−thiolate structures influence the formation of Au−Cu nanoparticle alloys, we compared the bimetallic nanoparticle products obtained from our one-phase, aqueous synthesis described above to a standard, two-phase Brust−Schiffrin synthesis (2PBSS).[25] This comparison is useful because multiple groups have demonstrated that in the 2PBSS metal−thiolate bonds do not form prior to introduction of reducing agent and subsequent NP nucleation.[26,30,31] Therefore, if the mixed-metal thiolate species we describe are important for alloy formation, one will observe significant differences in the final NP composition architecture (e.g., alloy vs core−shell motifs) depending upon whether a one- or two-phase synthesis is used. (We note that while it is obvious that two different preparations may yield two different products, these syntheses share significant similarity (vide infra). By exploiting their fundamental difference—the presence or absence of metal−thiolate prenucleation species, we target the chemical underpinnings of these differences both in the current report and in all Brust−Schiffrin derived syntheses.)

In order to facilitate comparison between our observations and previous work on two-phase syntheses, we compared 1D ^1H NMR and ^1H diffusion measurements of the prenucleation species present in a traditional 2PBSS in toluene to the prenucleation species observed in an analogous one-phase Brust−Schiffrin synthesis using a 50:50 Au:Cu initial metal ion ratio (Figure 3a). In these controls, dodecanethiol rather than PEGSH serves as the capping ligand, and the phase transfer agent, TOAB, is present in both the 2PBSS and "one-phase" analogue in ethanol (to ensure solubility of all reagents).

Consistent with previous reports,[26,30] ^1H NMR and diffusion measurements of the 2PBSS prenucleation species revealed that no metal−sulfur bonds were formed prior to $NaBH_4$ addition (Figure 3). Instead, metal halide anions coordinate to the ammonium headgroups on the $[TOA]^+$ inverse micelle as indicated by the chemical shift change of the nearby resonances, indicating fast anion exchange between the metal halide complexes and free halides. Further, in the case of the paramagnetic metal precursor, Cu(II), distance-dependent ^1H signal dephasing[32,33] is observed for resonances closest to the quaternary ammonium (Figure 3a). This distance-dependent dephasing is apparent from the broadening of the resonances closest to the quaternary ammonium, whereas the terminal methyl remains narrow, consistent with the formation of an encapsulating, inverse micelle structure.[34]

DOI: 10.1021/jacs.5b10124
J. Am. Chem. Soc. 2015, 137, 15852−15858

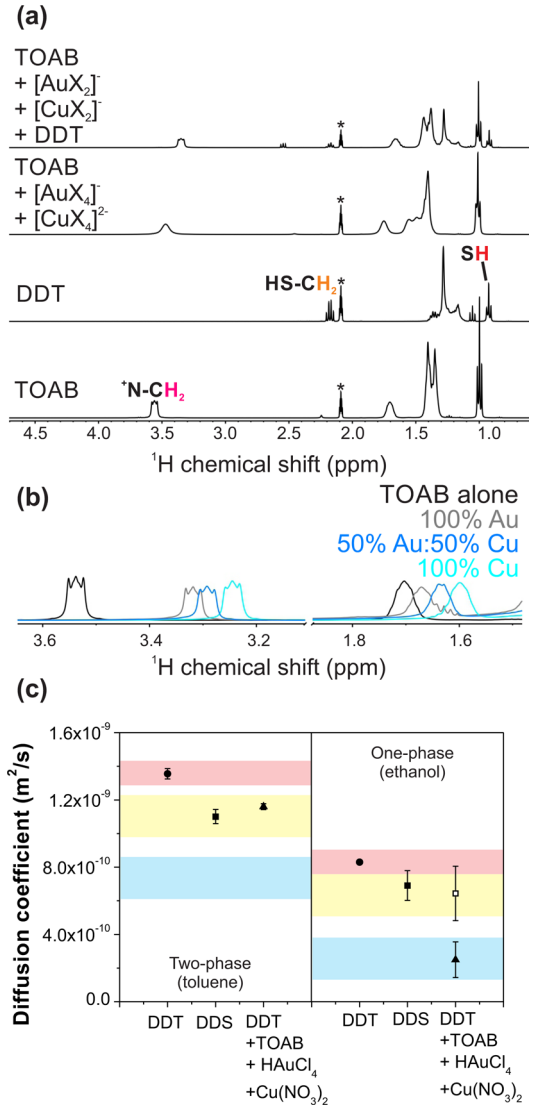

Figure 3. (a) ^{1}H NMR spectra comparison of TOAB, DDT, TOAB + $[AuX_4]^-$ + $[CuX_4]^{2-}$, and TOAB + $[AuX_2]^-$ + $[CuX_2]^-$ + DDT recorded at 14.1 T and 25 °C. Asterisk denotes residual solvent signal. (b) ^{1}H NMR spectra depicting the shift in protons both one (δ = 3.6–3.2 ppm) and two positions (δ = 1.8–1.5 ppm) away from the quaternary ammonium as the counterion on TOA^+ is changed from Br^- (black) to a mixture of Br^- and $[AuX_2]^-$ (gray), a combination of $[AuX_2]^-$ and $[CuX_2]^-$ (blue), or $[CuX_2]^-$ (cyan). (c) The left column shows diffusion coefficients of the species present in a typical two-phase synthesis shown in the top spectra of (a) while the right column depicts the diffusion coefficients present in solution for the same species in deuterated ethanol (one-phase synthesis analogue) obtained via integration of the DDT ^{1}H resonances $(CH_2)_n$, n = 2–10, at δ = 1.3 ppm. NB: differences observed in diffusion coefficients for the same molecules (e.g., DDT alone) are a result of the difference in solvent viscosities.

Upon addition of DDT, the signal dephasing is eliminated in reaction mixtures containing Cu, indicating that the Cu(II) in these micelles has been reduced to diamagnetic Cu(I) (Figure 3a). The increased spectral resolution after the addition of DDT allows anion composition on the micelle interior to be determined. Comparison between three reaction mixtures—100% Au, 50:50 Au:Cu, and 100% Cu—shows a gradual shift in the ^{1}H resonance adjacent to the quaternary ammonium, suggesting a change in anion composition inside the micelle (Figure 3b). This observation is consistent with micelles that contain both metals but do not form larger metal–thiolate structures like those observed in either one-phase synthesis.

Comparison of the ^{1}H diffusion coefficients of the $(CH_2)_n$ (n = 2–10) ^{1}H resonances on the DDT ligand shows a dramatic difference between one- and two-phase preparations (Figure 3c). No larger thiolate structures are detected in a two-phase toluene synthesis, but in a one-phase analogue, larger thiolates are observed, as they are in the one-phase aqueous synthesis (*vide supra*). Indeed, over the course of the experiment, a white precipitate was observed in the ethanol reaction mixtures, but not in the toluene mixtures, as would be expected in the formation of metal–thiolate coordination polymers (for expanded discussion on the formation and isolation of metal–thiolate structures see Supporting Information).

Resulting Nanoparticle Composition Architectures Are Different between the Two Methods. In the one-phase synthesis, structures consistent with alloyed NPs are obtained. In the two-phase synthesis, XAS and XPS data indicate that metal-segregated NPs are formed. For all preparation methods, final NP size, composition, and composition architecture were characterized by ICP-MS, STEM-EDS point spectra, HRTEM, XAS, XPS, PFG-SE NMR, and Auger electron spectroscopy (AES) (Figure 4, Figures S21–S31).

Particle diameters were consistent between one- and two-phase methods, and on average, core diameters were ~1.9 ± 0.2 nm. EXAFS comparison of low-Cu content NPs from the one- (14% Cu) and two-phase (12% Cu) syntheses showed differences in the spatial distribution of Cu atoms within the NP depending on synthetic route (Figure 4, Table 1). One-phase AuNPs exhibited a short Au–Au bond length from the relatively small size of the Au core (2.2 ± 0.5 nm) and a high Au–S CN, suggesting dense thiol coverage of the particle surface. Fitting results for one-phase Au_xCu_yNPs show a small amount of Au–Cu bonding from the Au L_3-edge (CN_{Au-Cu} = 0.30) and Cu K-edge (CN_{Cu-Au} = 1) EXAFS. The Au–Cu or Cu–Au bond distances range from 2.73 to 2.8 Å, indicating that Cu and Au are mixed in the nanoparticle core (Figure 5a). The difference in Au–Au CN between AuNPs and Au_xCu_yNPs prepared via the same one-phase method also supports the addition of Cu into the NP core.

Bonding at the surface of the one-phase NPs is also consistent with metal mixing. Au–S and Cu–S bond lengths and Au–S and Cu–S CN values indicate that both elements are present in the ligand layer. Interestingly, Au–S and Cu–S CN values are higher in the one-phase bimetallic case, as compared to the 100% AuNPs from the same preparation, which indicates possible changes in the metal–ligand binding motif, for example, from the "staple"[35,36] to "mount" motif.[20,37,38]

For the two-phase NPs, XAS analysis indicates metal segregated architectures. Au L_3-edge EXAFS fitting results show a slightly lower Au–Au CN for 100% AuNPs when compared to the Au–Au CN in the 50:50 Au_xCu_yNPs. The two-phase Au_xCu_yNPs show the presence of Cu primarily in the ligand layer, as indicated by the high Cu–S CN and absence of Au–Cu bonding from the Au L_3-edge EXAFS (Figure 5b). A longer Au–S bond of 2.43 Å and higher Au–Au CN indicate that less Au is found in the ligand layer. A small amount of intermetallic bonding could be resolved from the Cu K-edge, but not from the Au L_3-edge, likely due to the low concentration of these bonds and segregation of Au and

DOI: 10.1021/jacs.5b10124
J. Am. Chem. Soc. 2015, 137, 15852–15858

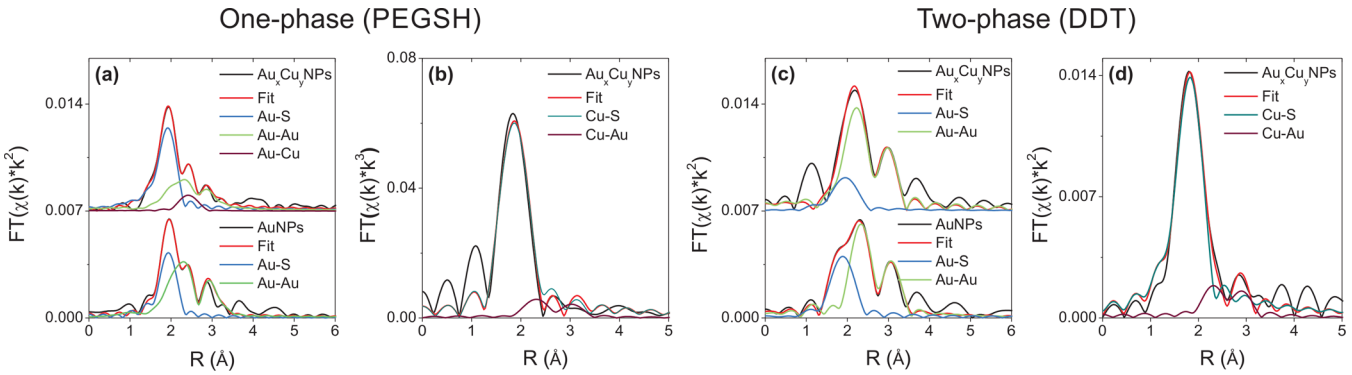

Figure 4. Fitted EXAFS spectra for one-phase Au- and Au_xCu_y-PEGSH NPs at the (a) Au L_3-edge and (b) Cu K-edge. Fitted EXAFS spectra for two-phase Au- and Au_xCu_y-DDT NPs at the (c) Au L_3-edge and (d) Cu K-edge.

Table 1. Au L_3-Edge and Cu K-Edge EXAFS Fitting Results for PEGSH- and DDT-Capped NPs

sample	path	CN	R (Å)	σ^2 (Å^2)	ΔE_0 (eV)
Au-PEGSH capped NPs	Au−S	0.6(1)	2.323(8)	0.003(1)	−1.5(9)
	Au−Au	7(1)	2.79(1)	0.015(1)	−1.5(9)
Au_xCu_y-PEGSH capped NPs (y = 14%)	Au−S	1.1(1)	2.327(8)	0.0040(6)	−0.7(4)
	Au−Au	3.5(7)	2.75(1)	0.011(3)	−0.7(4)
	Au−Cu	0.3(2)	2.73(2)	0.006(5)	−0.7(4)
	Cu−S	1.6(5)	2.27(3)	0.007(4)	−2(5)
	Cu−Au	1(1)	2.8(1)	0.01(1)	0(2)
Au-DDT capped NPs	Au−S	0.8(1)	2.334(5)	0.001(1)	1.4(7)
	Au−Au	5.8(5)	2.843(5)	0.0063(6)	1.4(7)
Au_xCu_y-DDT capped NPs (y = 12% Cu)	Au−S	0.8(4)	2.43(4)	0.005(4)	−1(2)
	Au−Au	7(3)	2.81(2)	0.007(4)	−1(2)
	Cu−S	2.5(3)	2.26(1)	0.007(1)	0(2)
	Cu−Au	1(1)	2.76(2)	0.007(7)	2(3)

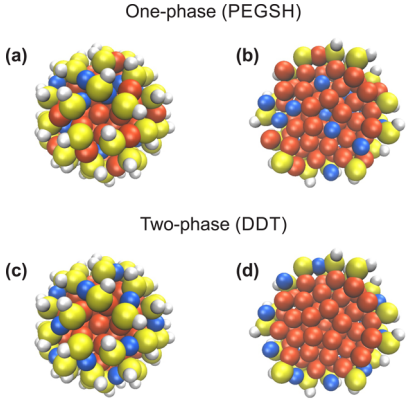

Figure 5. Cartoon of final nanoparticle architectures resulting from one-phase PEGSH (a, b) and two-phase DDT (c, d) syntheses. Full particles (a, c) and corresponding cross sections (b, d) are presented and illustrate differences in the spatial distribution of metal atoms resulting from the two approaches. Orange = Au, blue = Cu, yellow = S, and white = H. The ligands are represented as SH groups only, for clarity.

Cu—consistent with a single interface between Au and Cu in a core−shell motif.

The differences in particle morphology observed in XAS were also observed in high-resolution Cu 2p, Au 4f XPS spectra and Cu $L_3M_{45}M_{45}$ AES analysis as a function of various Au−Cu compositions. In all one-phase Au_xCu_yNPs, a binding energy shift in the Au $4f_{7/2}$ and Cu $2p_{3/2}$ peak is observed as a function of composition (Figures S21 and S25) and is a hallmark of alloying both at the nanoscale and in the bulk.[39] Further, Cu $L_3M_{45}M_{45}$ AES is consistent with the formation of small metal particles[40] and the presence of both elements distributed throughout the particle (Figure S22). The AES and XPS spectra were used to determine the modified Auger parameter for all NP compositions, which ranged from 1851.7 to 1850.0 eV (from 100% Cu to 10% Cu), generally decreasing with increasing Au content, also consistent with Au−Cu alloys.[41] In particular, 100% CuPEGSH-capped NPs exhibited two distinct peaks in the Cu $L_3M_{45}M_{45}$ AES spectra, with one Auger parameter consistent with metallic Cu (1851.7 eV) and one Auger parameter consistent with Cu−S bonds likely from the particle surface (1849.3 eV).

Conversely, XPS and AES analysis of the 2PBSS particles is consistent with metal segregation for all Au−Cu compositions. High-resolution XPS showed little to no binding energy shift for either the Au $4f_{7/2}$ or the Cu $2p_{3/2}$ regions as a function of composition (Figures S23 and S25). Cu $L_3M_{45}M_{45}$ AES peak position (modified Auger parameter is 1848.7 and 1849.6 eV, respectively) and line shape indicate that at both 12 and 24% Cu the majority of Cu is present in the ligand layer as Cu−S (Figure S24) (NB: the modified Auger parameter for a Cu_2S standard was measured at 1849.8 eV and is sensitive to nonstoichiometric phases.[42]) Indeed, for a particle of $d \sim 2$ nm and Cu concentrations of 12−21%, it is possible that all Cu atoms are located in the ligand shell.

As expected, when the % Cu is increased, Cu begins to migrate to the particle interior. In the Cu $L_3M_{45}M_{45}$ AES spectra of 42% Cu incorporation for a two-phase particle, two distinct peaks can be observed: one corresponding to Cu−S

DOI: 10.1021/jacs.5b10124
J. Am. Chem. Soc. 2015, 137, 15852−15858

and one corresponding to metallic Cu (modified Auger parameters of 1849.1 and 1850.7 eV, respectively; Figures S24 and S26).

CONCLUSIONS

In summary, we report a description of prenucleation species present in both one-phase and two-phase bimetallic NP syntheses. We find that one-phase syntheses form multinuclear metal−thiolate complexes and characterize these species using NMR, MS, XPS, and XAS techniques as well as by first-principles theoretical calculations. These mixed-metal prenucleation species are found to play a critical role in obtaining alloyed NPs of Au and Cu. Conversely, in two-phase syntheses, where metal−thiolate prenucleation species are not present, transition metal incorporation is likely dictated by the reduction rate of the original metal cation reagents and their aqueous species and results in the formation of core−shell architectures. Taken together, these data suggest that final atom positions within a NP may be tuned by manipulating the chemical structure of species present in the reaction prior to NP nucleation. Ultimately, these correlations point toward synthetic approaches that may achieve unprecedented control over multimetallic NP architectures.

ASSOCIATED CONTENT

Supporting Information

The Supporting Information is available free of charge on the ACS Publications website at DOI: 10.1021/jacs.5b10124.

XPS, AES, XAS, HRTEM, ICP-MS, DFT, and additional NMR used to characterize prenucleation species and final nanoparticles (PDF)

AUTHOR INFORMATION

Corresponding Author

*E-mail jem210@pitt.edu (J.E.M.).

Notes

The authors declare no competing financial interest.

ACKNOWLEDGMENTS

We thank Prof. Daniel Bain for the generous use of his ICP-MS. This work was supported by a National Science Foundation CAREER Award CHE-1253143, the Research Corporation for Science Advancement and the University of Pittsburgh. L.E.M. is supported by the Pittsburgh Quantum Institute (PQI) Graduate Fellowship. P.T.D. and G.M. acknowledge startup and Central Research Development funds (CRDF) from the University of Pittsburgh and the Center for Simulation and Modeling for computational support. O.S. was supported by a National Science Foundation REU fellowship (EEC-1359308). D.M.C. was supported by the NSERC CGS-Alexander Graham Bell scholarship, and P.Z. acknowledges the NSERC Discovery Grant. CLS@APS facilities (Sector 20) at the Advanced Photon Source (APS) are supported by the U.S. Department of Energy (DOE), NSERC Canada, the University of Washington, the CLS, and the APS. Use of the APS is supported by the DOE under Contract DE-AC02-06CH11357. MRCAT operations are supported by the DOE and MRCAT member institutions. This research used resources of the Advanced Photon Source, a DOE Office of Science User Facility operated for the DOE Office of Science by Argonne National Laboratory, under Contract DE-AC02-06CH11357.

REFERENCES

(1) Guidez, E. B.; Mäkinen, V.; Häkkinen, H.; Aikens, C. M. *J. Phys. Chem. C* **2012**, *116*, 20617.
(2) Hartmann, M. J.; Häkkinen, H.; Millstone, J. E.; Lambrecht, D. S. *J. Phys. Chem. C* **2015**, *119*, 8290.
(3) Yamazoe, S.; Kurashige, W.; Nobusada, K.; Negishi, Y.; Tsukuda, T. *J. Phys. Chem. C* **2014**, *118*, 25284.
(4) Zhang, L.; Anderson, R. M.; Crooks, R. M.; Henkelman, G. *Surf. Sci.* **2015**, *640*, 65.
(5) Cortie, M. B.; McDonagh, A. M. *Chem. Rev.* **2011**, *111*, 3713.
(6) Malola, S.; Lehtovaara, L.; Häkkinen, H. *J. Phys. Chem. C* **2014**, *118*, 20002.
(7) Riccardo, F. *J. Phys.: Condens. Matter* **2015**, *27*, 013003.
(8) Bhattarai, N.; Black, D. M.; Boppidi, S.; Khanal, S.; Bahena, D.; Tlahuice-Flores, A.; Bach, S. B. H.; Whetten, R. L.; Jose-Yacaman, M. *J. Phys. Chem. C* **2015**, *119*, 10935.
(9) Fields-Zinna, C. A.; Crowe, M. C.; Dass, A.; Weaver, J. E. F.; Murray, R. W. *Langmuir* **2009**, *25*, 7704.
(10) Jiang, D.-e.; Dai, S. *Inorg. Chem.* **2009**, *48*, 2720.
(11) Malola, S.; Hartmann, M. J.; Häkkinen, H. *J. Phys. Chem. Lett.* **2015**, *6*, 515.
(12) Qian, H.; Jiang, D.-e.; Li, G.; Gayathri, C.; Das, A.; Gil, R. R.; Jin, R. *J. Am. Chem. Soc.* **2012**, *134*, 16159.
(13) Simpson, C. A.; Farrow, C. L.; Tian, P.; Billinge, S. J. L.; Huffman, B. J.; Harkness, K. M.; Cliffel, D. E. *Inorg. Chem.* **2010**, *49*, 10858.
(14) Wuithschick, M.; Birnbaum, A.; Witte, S.; Sztucki, M.; Vainio, U.; Pinna, N.; Rademann, K.; Emmerling, F.; Kraehnert, R.; Polte, J. *ACS Nano* **2015**, *9*, 7052.
(15) Gary, D. C.; Terban, M. W.; Billinge, S. J. L.; Cossairt, B. M. *Chem. Mater.* **2015**, *27*, 1432.
(16) Essinger-Hileman, E. R.; DeCicco, D.; Bondi, J. F.; Schaak, R. E. *J. Mater. Chem.* **2011**, *21*, 11599.
(17) Marbella, L. E.; Andolina, C. M.; Smith, A. M.; Hartmann, M. J.; Dewar, A. C.; Johnston, K. A.; Daly, O. H.; Millstone, J. E. *Adv. Funct. Mater.* **2014**, *24*, 6532.
(18) Archer, P. I.; Santangelo, S. A.; Gamelin, D. R. *J. Am. Chem. Soc.* **2007**, *129*, 9808.
(19) Dharmaratne, A. C.; Dass, A. *Chem. Commun.* **2014**, *50*, 1722.
(20) Yang, H.; Wang, Y.; Yan, J.; Chen, X.; Zhang, X.; Häkkinen, H.; Zheng, N. *J. Am. Chem. Soc.* **2014**, *136*, 7197.
(21) He, R.; Wang, Y.-C.; Wang, X.; Wang, Z.; Liu, G.; Zhou, W.; Wen, L.; Li, Q.; Wang, X.; Chen, X.; Zeng, J.; Hou, J. G. *Nat. Commun.* **2014**, *5*, 4327.
(22) Motl, N. E.; Ewusi-Annan, E.; Sines, I. T.; Jensen, L.; Schaak, R. E. *J. Phys. Chem. C* **2010**, *114*, 19263.
(23) Straney, P. J.; Andolina, C. M.; Millstone, J. E. *Isr. J. Chem.* **2015**, DOI: 10.1002/ijch.201500033.
(24) Andolina, C. M.; Dewar, A. C.; Smith, A. M.; Marbella, L. E.; Hartmann, M. J.; Millstone, J. E. *J. Am. Chem. Soc.* **2013**, *135*, 5266.
(25) Brust, M.; Walker, M.; Bethell, D.; Schiffrin, D. J.; Whyman, R. *J. Chem. Soc., Chem. Commun.* **1994**, 801.
(26) Li, Y.; Zaluzhna, O.; Xu, B.; Gao, Y.; Modest, J. M.; Tong, Y. J. *J. Am. Chem. Soc.* **2011**, *133*, 2092.
(27) Freeman, F.; Angeletakis, C. N.; Maricich, T. J. *Org. Magn. Reson.* **1981**, *17*, 53.
(28) Holewinski, A.; Idrobo, J.-C.; Linic, S. *Nat. Chem.* **2014**, *6*, 828.
(29) McKone, J. R.; Sadtler, B. F.; Werlang, C. A.; Lewis, N. S.; Gray, H. B. *ACS Catal.* **2013**, *3*, 166.
(30) Goulet, P. J. G.; Lennox, R. B. *J. Am. Chem. Soc.* **2010**, *132*, 9582.
(31) Ohyama, J.; Teramura, K.; Higuchi, Y.; Shishido, T.; Hitomi, Y.; Kato, K.; Tanida, H.; Uruga, T.; Tanaka, T. *ChemPhysChem* **2011**, *12*, 127.
(32) Bloembergen, N. *J. Chem. Phys.* **1957**, *27*, 572.
(33) Solomon, I. *Phys. Rev.* **1955**, *99*, 559.
(34) Li, Y.; Zaluzhna, O.; Tong, Y. J. *Langmuir* **2011**, *27*, 7366.
(35) Heaven, M. W.; Dass, A.; White, P. S.; Holt, K. M.; Murray, R. W. *J. Am. Chem. Soc.* **2008**, *130*, 3754.

DOI: 10.1021/jacs.5b10124
J. Am. Chem. Soc. 2015, 137, 15852−15858

(36) Jadzinsky, P. D.; Calero, G.; Ackerson, C. J.; Bushnell, D. A.; Kornberg, R. D. *Science* **2007**, *318*, 430.
(37) Desireddy, A.; Conn, B. E.; Guo, J.; Yoon, B.; Barnett, R. N.; Monahan, B. M.; Kirschbaum, K.; Griffith, W. P.; Whetten, R. L.; Landman, U.; Bigioni, T. P. *Nature* **2013**, *501*, 399.
(38) Yang, H.; Wang, Y.; Huang, H.; Gell, L.; Lehtovaara, L.; Malola, S.; Häkkinen, H.; Zheng, N. *Nat. Commun.* **2013**, *4*, 2422.
(39) Santra, A. K.; Subbanna, G. N.; Rao, C. N. R. *Surf. Sci.* **1994**, *317*, 259.
(40) Vijayakrishnan, V.; Rao, C. N. R. *Surf. Sci.* **1991**, *255*, L516.
(41) Toshima, N.; Wang, Y. *Langmuir* **1994**, *10*, 4574.
(42) Manisha, K.; Tsuyoshi, H.; Kazuya, T.; Kazuhiro, Y.; Masakazu, A. *Sci. Technol. Adv. Mater.* **2008**, *9*, 035011.

DOI: 10.1021/jacs.5b10124
J. Am. Chem. Soc. 2015, 137, 15852−15858